Transcranial Ultrasound and Magnetic Resonance Image Fusion With Virtual Navigator

Maria Marcella Laganà, Maria Giulia Preti, Leonardo Forzoni, Sara D'Onofrio, Stefano De Beni, Antonello Barberio, Pietro Cecconi, and Giuseppe Baselli

***Abstract*—The Virtual Navigator (VN) technology was used for the fusion of transcranial Ultrasound (US) and brain Magnetic Resonance Images (MRI), with a repeatability error under 0.1 cm. The superimposition of US to the previously acquired MRI volume consisted of external point-based registration, that was subsequently refined with image-based registration of internal brain structures. The common registration procedure with the usage of external fiducial markers acquired with the two modalities was improved using facial anatomical landmarks, with a reduction of the internal targeted structure residual shift (maximum 0.7 cm in the cranio-caudal direction). This allowed the investigation of Deep Cerebral Veins and dural sinuses insonated from the condyloid process of the mandible, a recently introduced US window. The fusion of these vessels to the MRI volume provided their anatomical position and helped excluding false Doppler signal sources.**

***Index Terms*—Fusion imaging, image registration, magnetic resonance imaging, transcranial ultrasound, virtual navigator.**

I. Introduction

THE fusion between Ultrasound (US) images and other diagnostic images like Computed Tomography (CT) or Magnetic Resonance Imaging (MRI) allows to integrate the 2D real-time anatomical and functional information provided by US into a 3D anatomical context of higher precision and, via these images, with functional information given by other imaging modalities (CT/MRI angiography, emission tomography, other MRI modalities, etc.). This can be obtained through the Virtual Navigator (VN) technology, which is widely used in diagnostic and interventional procedures, especially in the liver [1]–[4] and in prostate [5], as well as for a better localization of tumors [6] and bone landmarks in osteoarthritis [7].

Manuscript received April 16, 2012; revised October 09, 2012; accepted November 26, 2012. Date of publication February 01, 2013; date of current version July 15, 2013. The associate editor coordinating the review of this manuscript and approving it for publication was Prof. Dimitri Van De Ville.

M. M. Laganà, A. Barberio, and P. Cecconi are with the Fondazione Don Carlo Gnocchi ONLUS, 66-20148 Milan, Italy (e-mail: mlagana@dongnocchi.it).

M. G. Preti is with the Dipartimento di Bioingegneria, Politecnico di Milano. 32-20133 Milano, Italy. She is also with the Fondazione Don Carlo Gnocchi ONLUS, IRCCS S. Maria Nascente, 66-20148 Milan, Italy (e-mail: gpreti@dongnocchi.it).

L. Forzoni, S. D'Onofrio, and S. De Beni are with ESAOTE S.p.A., 58-16153 Genova, Italy (e-mail: leonardo.forzoni@esaote.com; sara.donofrio@esaote.com; stefano.debeni@esaote.com).

G. Baselli is with the Dipartimento di Bioingegneria, Politecnico di Milano, 32-20133 Milano, Italy (e-mail: giuseppe.baselli@polimi.it).

Color versions of one or more of the figures in this paper are available online at http://ieeexplore.ieee.org.

Digital Object Identifier 10.1109/TMM.2013.2244871

The VN has been recently extended to the investigation of head and neck vascular bed, both arterial [8], [9] and venous [10]–[12]. The transcranial Color Doppler (TCCD), developed in the 1980s, has been mainly used in arterial evaluations; there are some studies about veins in the 1990s and about the systematic descriptions of insonation methods and normal velocity ranges in vessels by Stolz and colleagues [13]–[16]. TCCD examinations of the veins regard the diagnosis and monitoring of patients with cerebral venous thrombosis [16] and stroke [17]; still, the radiological methods commonly used during the acute phases are MRI and CT venography. The difficulties found in the TCCD for venous investigation are the low spatial resolution, the low venous blood velocity and the high anatomic variability of intracranial venous vessels. Recently, the interest in the cerebral venous system has grown because of the supposed relationship between an abnormal extra- and intra-cranial venous condition, either morphological or functional, called chronic cerebrospinal venous insufficiency (CCSVI), and Multiple Sclerosis (MS) [18]–[20]. For the CCSVI diagnosis, a new transcranial US window, i.e. the condyloid process of the mandible (Fig. 1), has been defined [21] and used for the investigation of the deep cerebral veins and sinuses (Fig. 2). This new approach, different from the conventional transcranial US windows [22], was recently validated through VN and MRI as anatomical reference [10], [23]. The common technical difficulties of transcranial examination of deep cerebral veins and sinuses are increased for the vessels targeted by the condylar window, because of their morphology, location, and flow characteristics. Indeed, they are located at 6–8 cm from the ultrasound probe, they are thin (diameter about 2–4 mm), and run parallel to the skull. Further, their flow is slow (0.10–0.40 m/s) [22] and affected by the respiratory phase (i.e. usually activated or increased during inspiration). Finally the US beam, constrained to the narrow transcranial window of the mandible condyloid process, is almost orthogonal to the flow, thus severely limiting TCCD sensitivity unless proper beam steering strategies are applied. As to the last issue, the recently developed Directional Multigate Quality Doppler Profiles (QDP) technology [24]–[29] can be used in order to highlight the flow direction in real-time. In this paper we describe technical and practical methods for transcranial US and TCCD fusion on brain MRI with the use of VN. We point out the value of VN for intracranial venous measures and evaluations, especially for the condylar window, where the examination is difficult due to the lack of parenchymal references.

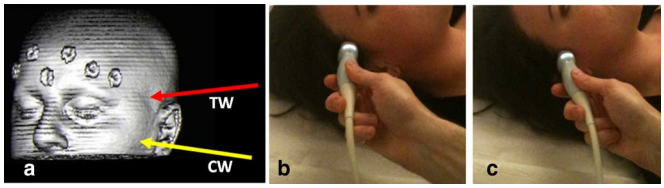

Fig. 1. Rendering of proton density MRI (a), with arrows pointing the temporal and condylar windows. Probe position for the US examination through temporal (b) and condylar (c) windows.

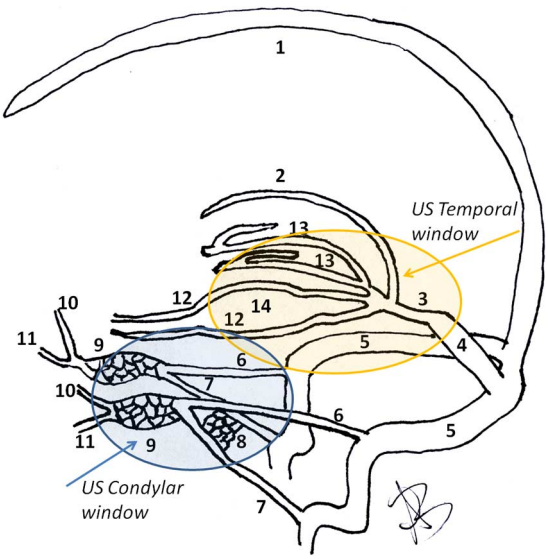

Fig. 2. Deep cerebral veins and dural sinuses: mutual positions and targeting from the different transcranial US windows. 1=Superior Sagittal sinus; 2=Inferior Sagittal Sinus; 3=Galen Vein; 4=straight sinus; 5=Transverse Sinus; 6=Superior Petrosal Sinus; 7=Inferior Petrosal Sinus; 8=Basilar Plexus; 9=Cavernous Sinus; 10= Superior Ophthalmic Vein; 11= Inferior Ophthalmic Vein; 12=Basal Vein of Rosenthal; 13=Internal Cerebral Vein. The midbrain (located at (14)) is surrounded by the Basal Vein of Rosenthal, it is well-visible by the transcranial window, and it is used as internal landmark reference for the second step of registration.

II. Materials and Methods

A. Subjects

MR and TCCD scans were acquired from two groups of subjects: group 1) 10 volunteers (mean age $=$ 35, range $=$ [27 $-$ 49], 5 males and 5 females); group 2) 24 volunteers (mean age $=$ 34, range $=$ [22 $-$ 56], 10 males and 14 females). The second group was used for a sub-study, where the performances of two registration methods were compared. All the participants were asked to sign an informed written consent and their capability of taking a prolonged inspiration without any head movement was assessed prior to their inclusion in the study. Further, a specific head support was used in both acquisitions in order to increase the comfort and so to avoid head movements during the examinations.

B. Data Acquisition

Prior to MRI and TCCD acquisitions, six multi-modality, conical design fiducial markers (PinPoint, Beekley, Medical, Bristol, USA) with a 1.27 mm diameter center hole were

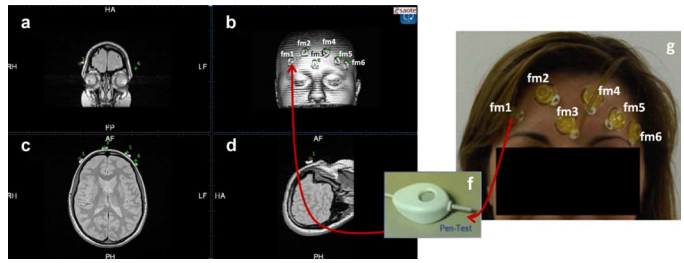

Fig. 3. Registration: step 1. First phase: pointing of the corresponding fiducial marker both in the Proton Density MRI 3D rendering (b), with the 3 main planes as reference (coronal -a-, axial -c-, sagittal -d-) and on the subject's forehead (g) laying in the bed before US examination. Registration pen shown in (f).

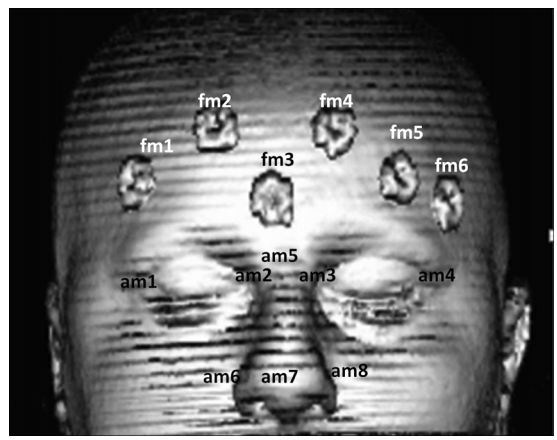

Fig. 4. Example of external fiducial markers (fm) and anatomical facial markers (am) positions.

placed on the subjects' forehead (Fig. 3(g) and Fig. 4), paying attention to position them on different planes, thanks to the natural curvature of the forehead.

MRI acquisitions were performed using a 1.5 T scanner (Siemens Magnetom Avanto, Erlangen, Germany), with a maximum gradient strength of 33 mT/m and a slew rate of 125 mT/m/ms, using standard 12-channels matrix head coil. The head was maintained as fixed as possible with the aid of two cushions, positioned between each ear and the coil. The following sequences were acquired: I) Scout T1 sequence: three sagittal slices, three coronal slices and one axial slice with low resolution (voxel size $= 2.2 \times 1.1 \times 6$ mm), used for positioning and orientation of the other sequences. II) axial Proton Density turbo spin echo, with the following parameters: TR $= 3270$ ms, TE $=$ 32 ms; echo train length $=$ 5; flip angle $=$ 150°, slice thickness $=$ 1.5 mm, matrix size $= 256 \times 256$, interpolated to 512×512, and Field of View (FOV) $= 250 \times 250$ mm. A slab of 100 slices without gap (thickness $=$ 150 mm) was acquired, the central slice of the slab was positioned parallel to the line that joins the inferior-anterior and inferior-posterior edge of the corpus callosum [30], visible on the sagittal scout T1. This standard positioning guaranteed the inclusion of the whole brain and the skin with the 6 fiducial markers.

TCCD acquisitions were performed by an Esaote US system (MyLabTwice, Esaote S.p.A., Genova-Italy), equipped with a Phased Array probe (PA240, Esaote; Operating Bandwidth: 1–4 MHz; B-Modes Frequencies: 2.0-2.5-3.3 MHz; Doppler

Frequencies: 1.6-2.0-2.5 MHz) and with the Virtual Navigation option [31]. The VN unit had an electromagnetic tracking system, consisting in a transmitter on a fixed position (close to the head of the volunteer) and a small receiver mounted on the US probe through a reusable tracking bracket (639-039, CIVCO Medical Solutions, Kalona, Iowa, USA). The transmitter, whose position was considered the origin of the reference system, was kept steady and correctly oriented toward the patient's head by a proper support, while the receiver provided the position and orientation of the US probe in the 3D space, in the system of reference given by the transmitter. The electromagnetic tracking system generates a magnetic field which has the highest magnitude in the position of the transmitter, and decreases at increasing distance. The magnetic field is lower than the Earth's magnetic field at 28 cm from the transmitter, so the latter was positioned at a distance of 10 cm from the subject head. The Proton Density weighted MR images were transferred in DICOM format to the US system through a DVD media support and the rendering of the skin and fiducial markers were performed.

C. Registration Procedure With Fiducial Marker

For each subject of the study, the registration procedure of US space to MRI space included two steps: step 1) a semi-automatic point-based rigid registration of corresponding fiducial markers; step 2) a manual (image based) fine tuning, based on anatomical landmarks localized on the basis of the previous coarse registration.

Step 1) The first registration step consisted on a manual and an automatic phase. As regards the first one, the fiducial markers on the MRI rendering and those on the subject laying in the bed for US examination had to be manually identified, for recording their coordinates in the two systems of reference and for establishing the correct correspondence between them. Finally, the registration matrix between the two stereotaxic spaces was automatically computed by the VN tool, using the markers coordinates in the two systems. More in practical detail, the first phase consisted on locating the external fiducial markers on the subject's forehead (Fig. 3, right): the coordinates of every fiducial marker in the ultrasound system of reference (Ppen) were obtained with a registration pen equipped with the electromagnetic receiver (Fig. 3, middle). In the same order, each marker was also located in the MR image reference system: the markers were manually identified on the 3D Proton Density rendering to collect their coordinates ($\mathrm{P_{MR}}$). Given the pairs of corresponding coordinates in the two systems of reference (ultrasound and MRI), in the second phase the registration matrix (Mreg) was computed by minimizing the following root mean square error (RMSE):

$$\mathrm{RMSE} = \sqrt{\frac{\sum_{\mathrm{i}=1}^{\mathrm{n}} \left(\mathrm{M_{reg}} * \mathrm{P_{pen_i}} - \mathrm{P_{MR_i}}\right)^2}{\mathrm{n}}}$$

where i indicates the considered fiducial marker and n the total number of markers, in our work equal to 6. The Mreg matrix transforms the 3D coordinates from ultrasound to MRI space, with 6 degrees of freedom (3 for translation and 3 for rotation). The registration matrix was computed applying a brute force approach, until RMSE resulted under 0.5 cm.

Step 2) The registration of the US image to the MRI was then improved with a manual fine tuning, aiming at reducing the misalignment between the MRI and the registered (with Mreg) US image, particularly in the internal structures, near the vessels which will be investigated. Indeed, a minimum shift between the external fiducial markers on the two imaging modalities could cause a higher internal shift, that we want to minimize. This was obtained by selecting structures which are well enhanced in both the image modalities, due to either anatomical or hemodynamic contrast, and manually reducing their mutual shift. The internal structures considered for the image-based registration were: the third ventricle and the mid brain visualized with B-mode US from the temporal window, the Circle of Willis and the Middle Cerebral and Posterior Cerebral arteries, visualized with CD from the temporal transcranial window (Fig. 1); bone structures (the petrous apex and the sphenoid bone), insonated through the condylar window. The procedure required the user to identify the anatomical landmark on the 2D B-mode or CD US and to manually match it with the corresponding structure in MRI, freezing and manually shifting the US plane on the MR image until no residual shift was observed. This procedure was repeated for different scan orientations in order to guarantee a good match in the 3D space.

After the registration, for any probe position/orientation, the VN system gave the corresponding MRI slice, obtained by re-slicing the volume according to the current US insonation plane.

Before starting the US examination, the system repeatability error was tested: the same fiducial marker coordinates were measured twice using a registration pen with two different spatial orientations. Repeatability errors lower than 0.2 cm were considered acceptable.

D. Comparison of Registration Procedures With Fiducial Marker vs. Facial Landmarks

A further study for future protocols without external markers or retrospective exploitation of MRI was performed on the 24 volunteers of group 2. The first registration step was repeated with anatomical facial landmarks (Fig. 4) instead of fiducial markers, then the goodness of the registration was compared with the one obtained with the original approach. As shown in Fig. 4, four anatomical landmarks at the sides of the eyes, one in the middle of the eyes, one on the tip of the nose and two on the nose sides were considered (Fig. 4) as facial landmarks.

The comparison between the performances of the two registration procedures was based on the evaluation of the residual shift of the external markers, i.e. fiducial registration error, and

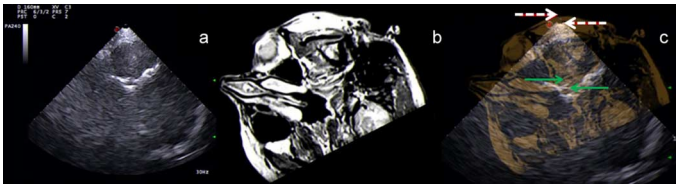

Fig. 5. (a) Example of US image, insonation from the condylar window; (b) MR oblique section corresponding to the US image after the first registration step; (c) fusion of (a) and (b). The example shows how to check the fiducial and target registration errors after the step 1 of registration with fiducial markers: an external and internal (sphenoid bone) lateral shift of 0.3 cm are visible in the axial plane (dotted arrows and continuous arrows respectively).

of the internal landmarks (mid brain, petrous apex, sphenoid bone, middle and posterior cerebral arteries), i.e. target registration error, visualized by US and MRI, prior to the second step of the registration process. The residual target registration error is the most critical, since it is the residual shift of the two imaging modalities near the area of interest for our examinations and it is the one that has to be manually corrected with the second step of the registration.

E. Transcranial ECD Examination and Navigation Procedures

Fusion imaging procedure with VN was performed in supine posture (0° tilt). Non-metallic beds were used to avoid interference with the electromagnetic VN system. TCCD examinations were performed by an expert sonographer (more than 20 years of experience in US examination) trained for the US venous transcranial evaluations through temporal and condylar windows (3 years of experience for this new approach). Each subject underwent trans-condylar TCCD evaluation at the level of the condyloid process of the mandible (Fig. 1(b)). In order to assess errors introduced by the conventional blind TCCD examination without VN embedded on US system, the DCV targeting and CD evaluation procedures were performed with the MRI frame switched off, thus based on the sole B-mode. If no signal was detectable due to low flow velocity, the subject was asked to take a prolonged and deep inspiration, with the maximum duration he/she was capable to take, in order to increase the venous flow velocity [32] and to be able to locate the addressed vein with CD signal. If neither this was successful for finding the vessel of interest, it was considered not seen. Finally, the MRI volume was switched on and the anatomical position of the targeted vessel was assessed and confirmed with the color Doppler fusion with MRI.

III. Results

The system repeatability error measured with the registration pen was always under 0.1 cm.

A. Registration Quality With Fiducial Markers

For all the performed examinations, the registration error obtained after the first step of the coregistration process was below 0.5 cm. An example of the residual external and internal shift after the step 1 of the registration with fiducial markers is shown in Fig. 5.

Examples of the final registration performance (using fiducial marker and image-based refinement) are shown in Figs. 6(a), 7, and 8, where the fusion of the midbrain (Fig. 6(a)) and of the middle (Fig. 7) and posterior cerebral arteries (Fig. 8) are representing the good internal matching between the two imaging modalities.

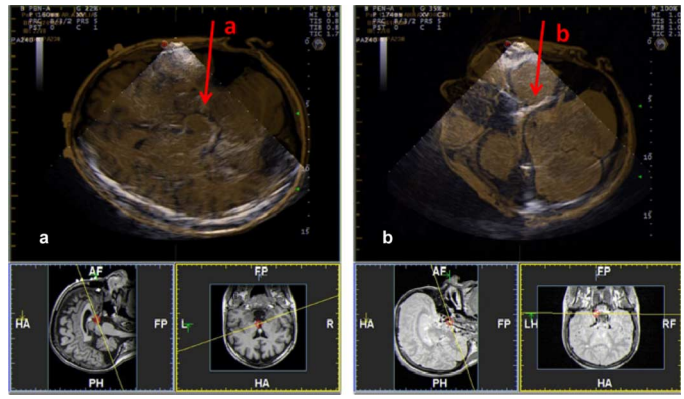

Fig. 6. Midbrain (a) and sphenoid bone (b) visualized with the two imaging modalities. Their fusion gives information about a good internal registration quality. In both examples there is a perfect matching, i.e. zero visible shift of the internal structure of interest visualized with the two imaging modalities. The first one resulted after the registration with fiducial markers, followed by a 0.6 cm lateral manual shift of the US in the axial plane and 0.7 cm in the cranial direction; the second one resulted after the registration with facial landmarks and then by a 0.3 cm lateral manual shift of the US in the axial plane.

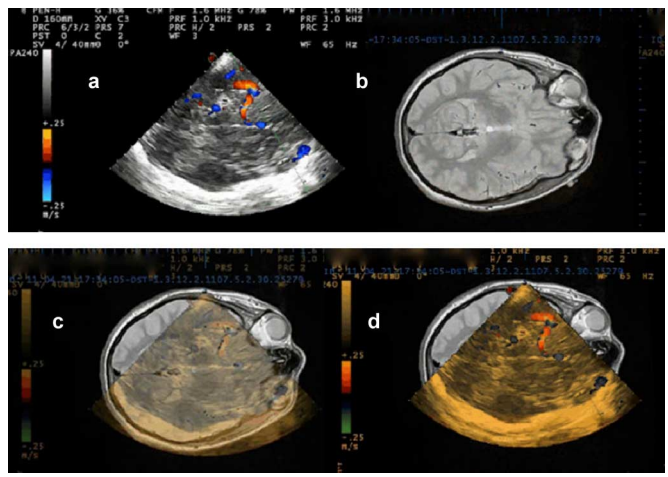

Fig. 7. Internal vessel landmarks (middle cerebral artery) used for the manual registration adjustment and for checking the final registration quality. The US image is shown in (a), the MRI is shown in (b) and the fusion is shown in (c) and (d) with progressive decrement of US transparence. The current matching of the middle cerebral artery resulted after a registration with fiducial markers, followed by a 0.4 cm lateral manual shift of the US in the axial plane and 0.5 cm in the caudal direction.

B. Comparison of Registration Quality With Fiducial Marker vs. Facial Landmarks

As regards the comparison between the two different registration procedures performed on the 24 volunteers of group 2, with both the approaches (fiducial markers and the facial landmarks) the registration error obtained after the first step of the coregistration process was below 0.5 cm. Different target registration errors were observed: with the fiducial marker approach we observed an average craniocaudal shift of internal structures of 1 cm (range 0.5–2 cm), an average lateral shift of 1 cm (range

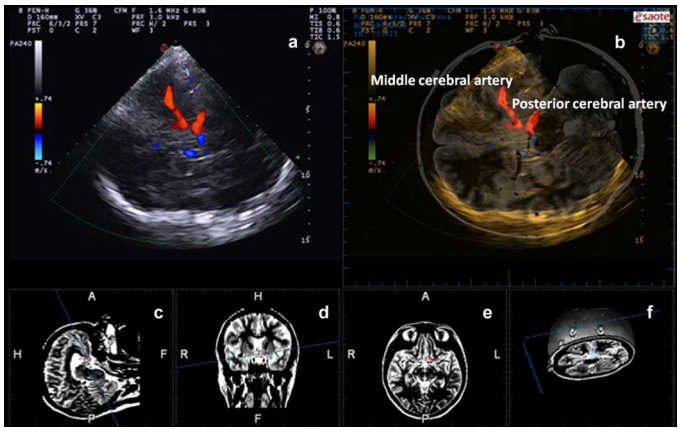

Fig. 8. (a) Middle and posterior cerebral arteries visualization in the US and (b) their fusion to MRI volume, as internal anatomical confirmation of the correct coregistration between US and MRI. The insonation plane orientation is visualized on (c) sagittal, (d) coronal and (e) axial views; (f) cut MRI rendering corresponding to the current US insonation plane. The matching of the middle and posterior cerebral arteries was obtained after a registration with facial landmarks, followed by a 0.3 cm lateral manual shift of the US in the axial plane and 0.4 cm in the cranial direction.

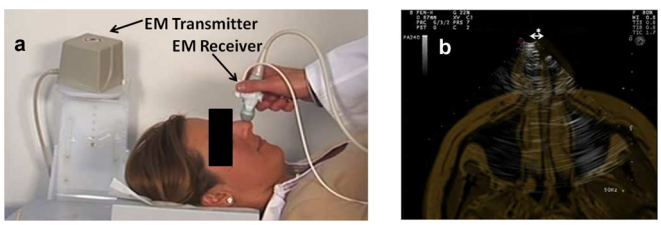

Fig. 9. The electromagnetic system is shown in (a): it consists on an electromagnetic transmitter, fixed on the bed at 10 cm from the subject head, and an electromagnetic receiver, mounted on the US probe, which provides its current position. The example displays how to check the facial landmark residual error after the first step of the registration: the nose top was pointed with the US probe (a) and the external residual shift between the two imaging modalities was assessed (-b-, on the axial plane it is possible to measure the lateral shift and the anterior-posterior shift, here respectively 0.35 cm and 0.1 cm).

0.5–1.5 cm) and an average antero-posterior shift of 0.3 cm (range 0.2–0.4 cm), whereas with the facial landmark approach the errors lowered to 0.5 cm (range 0–0.7 cm), 0.1 cm (range 0–0.5 cm) and 0.2 cm (range 0.1–0.3 cm) respectively.

Both of the semi-automatic registrations took a total time of 4 minutes, but the step 2 of the registration process was shorter after the registration with facial markers, since the smaller residual internal error facilitated the manual fine tuning: a mean of 3 minutes vs a mean of 2 minutes was required, respectively with the fiducial marker and with facial landmark approaches.

An example of the residual external shift after the step 1 of the registration with facial landmarks is shown in Fig. 9. An example of the final registration with the facial landmark approach and the manual tuning is shown in Fig. 6(b), where the image fusion of the sphenoid bone shows the internal goodness of the whole registration process.

C. Insonation Through the Condylar Window

When insonating through the transcranial window at the level of the condyloid process of the mandible, different cerebral veins were detectable (Fig. 2), by using different positioning (angles) of the probe and of the insonation plane. Through the

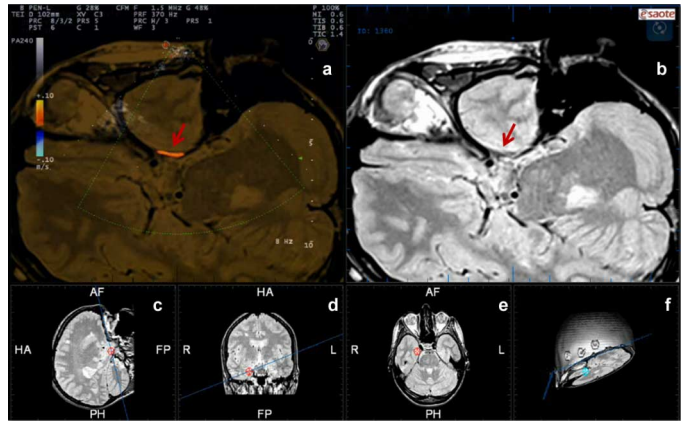

Fig. 10. Example of superior petrosal sinus insonation ipsilateral to the probe. (a) US fused with MRI; (b) MRI oblique plane; the vessel position is confirmed by the marker visualized on sagittal (c), coronal (d) and axial (e) views; (f) cut MRI rendering corresponding to the current US insonation plane.

fusion with the MRI volume and the navigation procedure, the structures identified with the US examination were: the Basilar Plexus, the Cavernous Sinus, the Superior Petrosal Sinus (Fig. 10), the Inferior Petrosal Sinus (Fig. 11), the first segment of the Basal Vein of Rosenthal (Fig. 12) and the ophthalmic vein (Fig. 13). The fusion imaging of US with MRI allowed to identify and recognize confounding US signals (in 21/34 subjects), i.e. CD signals which appeared similar to those coming from the petrosal or cavernous sinuses (Fig. 14). Confounding CD sources were probably due to the air vibration on the bone structures of the nasal cavity and their position outside the brain could be assessed on the three MRI planes of the VN (Fig. 15). It required about 10 minutes for each side in order to correctly image the intracranial vessels. If no vessel was visible, and the subject was required to take a prolonged inspiration, other 10 minutes were necessary. As to the main vessels supposed to be impaired in CCSVI, the Superior Petrosal Sinus was detected in 13/34 (38%) subjects and the Inferior Petrosal Sinus in 7/34 (21%) (Fig. 11). Interestingly, in 2/34 subjects also the Basal Vein of Rosenthal (Fig. 12) and the ophthalmic vein (Fig. 13) were observed.

IV. Discussion

While MRI is a valuable tool for the comprehensive anatomical 3D information within a wide FOV, US technology represents the best cost effective tool for real time assessment of the cerebral veins, but it is limited in its FOV by the head bones and a correct steering is not always sufficient to have the correct insonation angle to image blood flow without the mirror effect. The latter problem can be faced using QDP technology [24]–[29], while the restricted FOV and the lack of anatomical references when addressing deep vessels can be overcome with VN technology, providing anatomical references by another imaging modality (in our study the MRI), fused on the current US plane after the whole registration process. We chose to use Proton Density weighted MRI for many reasons: it allowed to visualize the fiducial markers needed for the registration (Fig. 3) and it contrasted the main intracranial veins from the surrounding brain tissue, allowing to validate the US results.

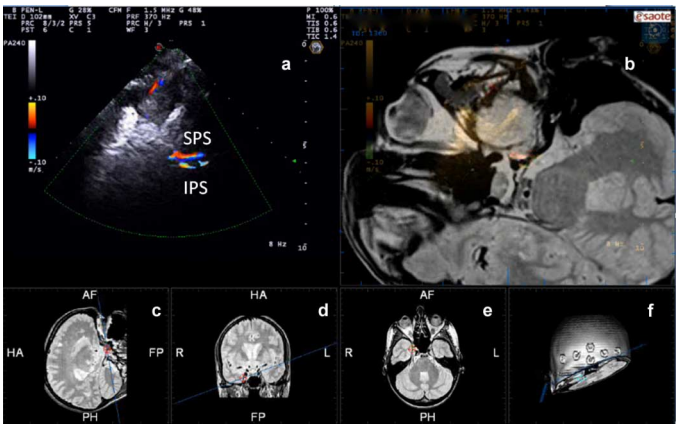

Fig. 11. Example of Superior Petrosal Sinus (SPS) and Inferior Petrosal Sinus (IPS) insonation. (a) US fused with MRI; (b) MRI oblique plane; the vessel position is confirmed by the marker visualized on sagittal (c), coronal (d) and axial (e) views; (f) cut MRI rendering corresponding to the current US insonation plane.

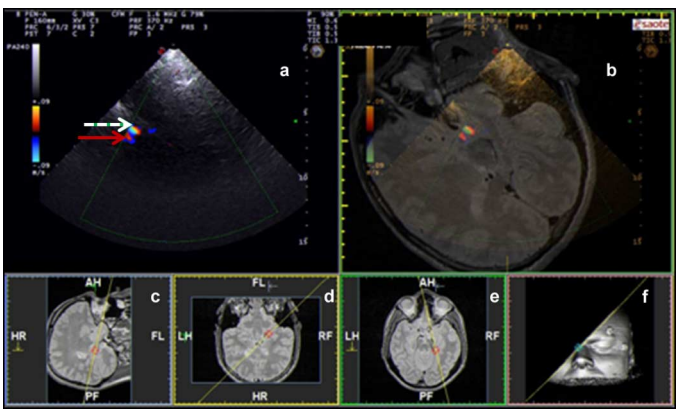

Fig. 12. Example of Superior Petrosal Sinus (dotted arrow) and first segment of Rosenthal Vein (continuous arrow). (a) US fused with MRI; (b) MRI oblique plane; the vessel position is confirmed by the marker visualized on sagittal (c), coronal (d) and axial (e) views; (f) cut MRI rendering corresponding to the current US insonation plane.

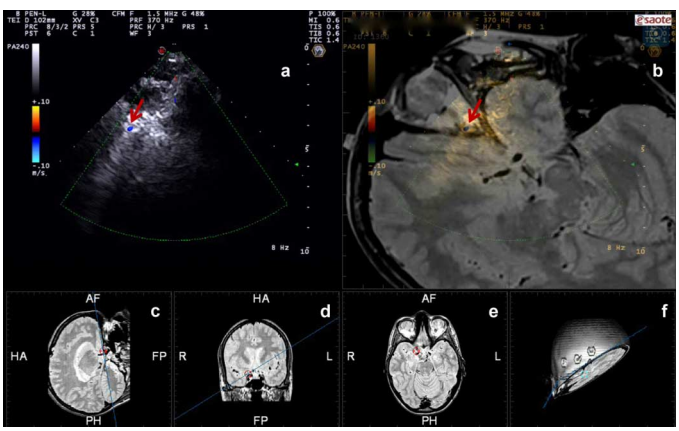

Fig. 13. Example of ophthalmic vein (pointed by the arrow) imaged through the condylar window. (a) US image; (b)US fused with MRI. The vessel position is confirmed by the marker visualized on sagittal (c), coronal (d) and axial (e) views; (f) cut MRI rendering corresponding to the current US insonation plane.

Since Proton Density MRI is also the optimal sequence for MS lesion localization and segmentation, it is likely to be a good reference frame for TCCD even in clinical cases were the relationship of deep cerebral veins and the surrounding

Fig. 14. False signals (a), (b) and real venous signal (c).

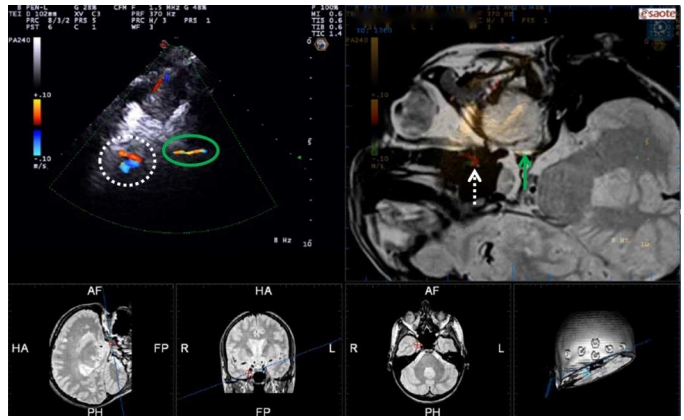

Fig. 15. An example of false signal and true signal (Superior petrosal sinus) in the same frame, and their anatomical position visualized on MRI. (a) US image with dotted and continuous circles pointing the false and the true signals respectively, (b) fused US and MR image with dotted and continuous arrows pointing the false and the true signal positions. The signal position has been pointed with a mark in the sagittal (c), coronal (d), axial (e) and oblique (f) sections.

white matter structures is investigated. The selected scan would permit precise lesion volume measures due to its high resolution ($\text{voxel size} = 0.49 \times 0.49 \times 1.5\ \text{mm}$). A further extension can be represented by the co-registration of US with additional MRIs with various functional and anatomical contrasts using Proton Density MRI as main reference, for example Susceptibility Weighted Imaging (SWI) [33], [34], Time of Flight (TOF) with contrast of the major vessels of interest.

In order to be sure to image the correct vessels of interest through transcranial windows without the help of the MRI, the sonographer has to use some references, as it is currently done with the midbrain for imaging the Basal vein of Rosenthal through the temporal window (scheme of Fig. 2). US through the condylar window is difficult due to the poor anatomical landmarks surrounding the vessels of interest (Fig. 14(c)) and to the high occurrence of confounding signals (Figs. 14(a) and (b), 15). A Color Doppler marker for the detection of the Cavernous sinus and Superior and Inferior petrosal sinuses, i.e. the “cloud of color”, is visible during a prolonged inspiration [29]. But this cloud of color, however, can be mimicked by the signals coming from the nasal bones (Fig. 15). As shown in this work, the fusion of the US with MRI volume created a complete high-quality portrait of the targeted intracranial vessels (Figs. 10–13), allowing to understand the relative position of Doppler signals associated to brain vessels, with respect to signals placed outside the brain.

Since the US examination is operator dependent, especially through the condylar window, we chose a single trained examiner: a higher inter-observer variability, in particular for trained

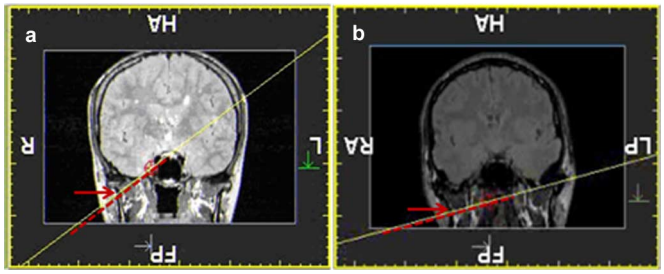

Fig. 16. Different insonation angles (between dotted lines and the arrows) from the condylar window. Correct US insonation plane for the petrosal sinuses insonation (a), wrong US insonation plane: the low angle gives US image out of the brain.

vs. non-trained examiners, but also for different trained examiners, compared to the intra-observer variability, was recently published [28]. The training for the transcranial insonation through this new approach is mandatory, indeed slightly different angles of the probe (Fig. 16) can image completely different areas of the examined subject's head, inside the brain (Superior Petrosal Sinus, Inferior Petrosal Sinus, Cavernous Sinus, Fig. 16(a)) or outside (Doppler signals detected in the nasal cavities area under the sphenoid sinus; Figs. 15, 16(b)), obtaining confounding signals in the last situation. Since the common (21/34 in our study) false signals are due to structures located near the vessels of interest, we tried to increase the performance of the registration process, especially aiming at the reduction of target registration errors. To this aim, we used a two-step registration method: the first one is semi-automatic and the second one is a final manual refinement. In the present work we reported fiducial repeatability errors on single external markers less than 0.1 cm and fiducial registration errors below 0.5 cm on the whole set of external markers. These corresponded to target registration errors on internal fiducial anatomical structures of maximum 2.0 cm and 0.7 cm (respectively for fiducial marker and facial landmark approach), which were manually reduced by a further registration fine tuning.

In literature, a recent study [35] reported an error of 0.35 mm due to the 3D localization of the probe and of 1.5 mm due to the calibration. The same study described a registration error of 1.5 mm in phantom studies but a higher registration error in clinical context (up to 10 mm). Another recent work, using facial landmarks, had precision, fiducial and target registration errors similar to ours [36]. Target registration errors of 0–2 mm in the falx and higher than 2 mm in the soft tissue have been shown in a intraoperative work using optical systems [37].

We tried to reduce the residual target error after the first registration step, comparing different approaches. The better performance of the registration procedure with facial anatomical landmarks, compared to the one obtained with applied fiducial markers, could be due to the proximity of these fiducial points (especially the ones of the eyes) to the internal target regions and to their higher dispersion in the 3D space. Indeed, their spatial cloud was better than the dispersion created by the curvature of the forehead for the applied fiducial marker, thus improving the point-based rigid registration. Moreover, applied markers are more sensitive to skin movements induced by the registration pen pressure. A good first registration phase allowed to accelerate the overall registration procedure, since it simplified the subsequent image-based fine tuning. Another and major advantage of the facial anatomical markers is the possibility to retrospectively use available clinical MRI volumes, with the only requirements of sufficient resolution and a FOV including the skin corresponding to the nose and the eyes. Furthermore, the absence of markers allows to acquire the MRI reference some days before the TCCD examination and even to use an initial MRI in several follow-up, if the brain anatomy is supposed to be stable between the two acquisitions.

As regards the second step of the coregistration process, it guaranteed a manual final refinement aiming at reducing to zero the shift of the same structure imaged with the two techniques. However, the refinement of the registration depended on the operator knowledge and skill in recognizing internal structures on US and MR and matching them. Anatomical landmarks surrounding the target were chosen, but the vessels of interest (deep cerebral veins and sinuses) were not used as targets for the manual tuning, in order to prevent a bias in the subsequent measurements.

Both the first and the second steps consisted on a rigid registration, since the same subject was imaged with the two technologies without brain changes between the two acquisitions.

After the two registration steps, the subject had to remain still for the whole transcranial US examination, which could last till 40 minutes. For this reason we provided a head support, which increased the comfort, but the head was not fixed. If during the examination we noticed the subject moving the head, we had to repeat at least the second step of the coregistration process. This did not happen often (3/34 cases), but smaller movements could occur. This limit has been overcame, as recently shown in a preliminary study [38], where we used a motion control sensor for compensating subject's movements in 3D TCCD application.

With the described procedures and accuracies, the US examination fused on a previously acquired MRI through VN technology can be used for different applications. We showed how it was fundamental for the validation of the veins targeted through the recently defined condylar window [10], [23]. Interestingly, this new approach allowed to image the Inferior Petrosal Sinus and the ophthalmic vein, that were not visible in the anatomical Proton Density weighted MRI, even if it confirmed the correct anatomical position. In particular, the possibility to image the ophthalmic vein by the condylar approach represents an interesting option for the study of the eye vessels hidden by the ocular bulb: the US insonation through the ocular bulb is possible in theory, but forbidden by health security rules. Further research application regards a wide and complete study about intracranial venous anatomy and hemodynamic, today limited to the vessels visible by the current insonation windows.

Another application of VN technology is the training, to improve the operator's experience and manual skill in the intracranial vessel examination, by means of delivering the fusion view during the vein targeting phase. For clinical research purposes the use of VN can objectify the addressed veins: without this technology their identification is prone to errors and it depends on the operator's experience [28].

Further extensions for the application of VN regard follow up studies and surgery, like recent studies showed [35], [36]. The described lower initial registration error with facial markers instead of fiducial markers and the consequent less need of manual tuning for the compensation of the mismatch between the two modalities images, show the possibility of using US and VN also with MRI acquired in a different day.

V. Conclusion

The present study on TCCD fusion with MRI, based on a VN technology embedded on a US system and an improved registration procedure, has allowed to insonate and identify deep brain veins, even those that are not detectable with the common used US windows. The proposed two step registration method, firstly based on external fiducial markers or facial landmarks, then on internal structures, demonstrated good applicability and precision. Indeed, the first step of the registration procedure was acceptable $(\mathrm{E} < 0.5\ \mathrm{cm})$ for all the subjects, the second step always reduced the registration error of internal structures to the minimum visible with human eyes and the precision of the system was always at least 0.1 cm. The registration outcomes based on facial landmarks strongly suggest the application of external fiducial markers be skipped, due to the higher simplicity, the possibility of a retrospective use of a previous reference MRI and the higher precision (maximum 0.7 cm in the craniocaudal direction) of the facial landmark approach. These analyses on deep cerebral veins bring further support to the use of a condylar window to access venous structures of clinical interest. Our results also confirm critical points on the evaluation of deep cerebral veins based on the sole US image anatomy, due to the difficulty in targeting the correct veins and in defining confounding Doppler sources.

Abbreviations

CCSVI	Chronic Cerebrospinal Venous Insufficiency
CT	Computer Tomography
FOV	Field Of View
MRI	Magnetic Resonance Imaging
MS	Multiple Sclerosis
QDP	Quality Doppler Profiles
SWI	Susceptibility Weighted Imaging
TCCD	Transcranial Color Doppler
TOF	Time of Flight
US	Ultrasound
VN	Virtual Navigator

Acknowledgment

The authors wish to thank G. Altobelli and L. Lodigiani (Esaote S.p.A., Italy) for the valuable contribution given to this work.

References

[1] L. Crocetti, R. Lencioni, S. Debeni, T. C. See, C. D. Pina, and C. Bartolozzi, "Targeting liver lesions for radiofrequency ablation: An experimental feasibility study using a CT-US fusion imaging system," *Invest. Radiol.*, vol. 43, pp. 33–39, Jan. 2008.

[2] D. A. Clevert, A. Helck, P. M. Paprottka, P. Zengel, C. Trumm, and M. F. Reiser, "Ultrasound-guided image fusion with computed tomography and magnetic resonance imaging. Clinical utility for imaging and interventional diagnostics of hepatic lesions," *Radiologe*, vol. 52, pp. 63–69, Jan. 2012.

[3] J. Rennert, M. Georgieva, A. G. Schreyer, W. Jung, C. Ross, C. Stroszczynski, and E. M. Jung, "Image fusion of contrast enhanced ultrasound (CEUS) with computed tomography (CT) or magnetic resonance imaging (MRI) using volume navigation for detection, characterization and planning of therapeutic interventions of liver tumors," *Clin. Hemorheol. Microcirc.*, vol. 49, pp. 67–81, 2011.

[4] Y. Kunishi, K. Numata, M. Morimoto, M. Okada, T. Kaneko, S. Maeda, and K. Tanaka, "Efficacy of fusion imaging combining sonography and hepatobiliary phase MRI with Gd-EOB-DTPA to detect small hepatocellular carcinoma," *AJR Amer. J. Roentgenol.*, vol. 198, pp. 106–114, Jan. 2012.

[5] O. Ukimura, M. M. Desai, S. Palmer, S. Valencerina, M. Gross, A. L. Abreu, M. Aron, and I. S. Gill, "3-Dimensional elastic registration system of prostate biopsy location by real-time 3-dimensional transrectal ultrasound guidance with magnetic resonance/transrectal ultrasound image fusion," *J. Urol.*, vol. 187, pp. 1080–1086, Mar. 2012.

[6] X. Lu, S. Suo, H. Liu, and S. Zhang, "Three-dimensional multimodal image non-rigid registration and fusion in a high intensity focused ultrasound system," *Comput. Aided Surg.*, vol. 17, pp. 1–12, 2012.

[7] A. Iagnocco, E. Filippucci, L. Riente, G. Meenagh, A. Delle Sedie, G. Sakellariou, F. Ceccarelli, C. Montecucco, S. Bombardieri, W. Grassi, and G. Valesini, "Ultrasound imaging for the rheumatologist XXXV. Sonographic assessment of the foot in patients with osteoarthritis," *Clin. Exp. Rheumatol.*, vol. 29, pp. 757–762, Sep.–Oct. 2011.

[8] L. Mercier, R. F. Del Maestro, K. Petrecca, A. Kochanowska, S. Drouin, C. X. Yan, A. L. Janke, S. J. Chen, and D. L. Collins, "New prototype neuronavigation system based on preoperative imaging and intraoperative freehand ultrasound: System description and validation," *Int. J. Comput. Assist. Radiol. Surg.*, vol. 6, pp. 507–522, Jul. 2011.

[9] G. Malferrari, M. Zedde, G. De Berti, M. Maggi, L. Lodigiani, and N. Marcello, "Virtual navigator study. Subset of preliminary data about arterial circulation," in *Proc. 16th Meeting of the European Society of Neurosonology and Cerebral Hemodynamics*, Munich, Germany, 2011, p. 67.

[10] P. Zamboni, E. Menegatti, G. Viselner, S. Morovic, and S. Bastianello, "Fusion imaging technology of the intracranial veins," *Phlebology*, Dec. 2011.

[11] M. Zedde, G. Malferrari, G. De Berti, M. Maggi, and L. Lodigiani, "Virtual navigator study. Subset of preliminary data about venous circulation," *Perspect. Med.*, 2012, 10.1016/j.premed.2012.02.008.

[12] M. Zedde, G. Malferrari, G. De Berti, M. Maggi, L. Lodigiani, and N. Marcello, "Virtual navigator study. Subset of preliminary data about venous circulation," in *Proc. 16th Meeting of the European Society of Neurosonology and Cerebral Hemodynamics*, Munich, Germany, 2011, p. 22.

[13] E. Stolz, S. S. Babacan, R. H. Bodeker, T. Gerriets, and M. Kaps, "Interobserver and intraobserver reliability of venous transcranial color-coded flow velocity measurements," *J. Neuroimag.*, vol. 11, pp. 385–392, Oct. 2001.

[14] E. Stolz, "Cerebral veins and sinuses," *Front. Neurol. Neurosci.*, vol. 21, pp. 182–193, 2006.

[15] E. Stolz, M. Kaps, and W. Dorndorf, "Assessment of intracranial venous hemodynamics in normal individuals and patients with cerebral venous thrombosis," *Stroke*, vol. 30, pp. 70–75, Jan. 1999.

[16] E. P. Stolz, "Role of ultrasound in diagnosis and management of cerebral vein and sinus thrombosis," *Front. Neurol. Neurosci.*, vol. 23, pp. 112–121, 2008.

[17] F. Schlachetzki, M. Herzberg, T. Holscher, M. Ertl, M. Zimmermann, K. P. Ittner, H. Pels, U. Bogdahn, and S. Boy, "Transcranial ultrasound from diagnosis to early stroke treatment—Part 2: Prehospital neurosonography in patients with acute stroke—The regensburg stroke mobile project," *Cerebrovasc. Dis.*, vol. 33, pp. 262–271, 2012.

[18] Y. Ge, V. M. Zohrabian, and R. I. Grossman, "Seven-Tesla magnetic resonance imaging: New vision of microvascular abnormalities in multiple sclerosis," *Arch. Neurol.*, vol. 65, pp. 812–816, Jun. 2008.

[19] Y. Ge, V. M. Zohrabian, E. O. Osa, J. Xu, H. Jaggi, J. Herbert, E. M. Haacke, and R. I. Grossman, "Diminished visibility of cerebral venous vasculature in multiple sclerosis by susceptibility-weighted imaging at 3.0 Tesla," *J. Magn. Reson. Imag.*, vol. 29, pp. 1190–1194, May 2009.
[20] B. Weir, "Multiple sclerosis—A vascular etiology?," *Can. J. Neurol. Sci.*, vol. 37, pp. 745–757, Nov. 2010.
[21] P. Zamboni, R. Galeotti, E. Menegatti, A. M. Malagoni, G. Tacconi, S. Dall'Ara, I. Bartolomei, and F. Salvi, "Chronic cerebrospinal venous insufficiency in patients with multiple sclerosis," *J. Neurol. Neurosurg. Psychiatry*, vol. 80, pp. 392–399, Apr. 2009.
[22] S. J. Schreiber, E. Stolz, and J. M. Valdueza, "Transcranial ultrasonography of cerebral veins and sinuses," *Eur. J. Ultrasound*, vol. 16, pp. 59–72, Nov. 2002.
[23] M. M. Lagana, L. Forzoni, S. Viotti, S. De Beni, G. Baselli, and P. Cecconi, "Assessment of the cerebral venous system from the transcondylar ultrasound window using virtual navigator technology and MRI," in *Proc. IEEE Eng. Med. Biol. Soc. Conf.*, 2011, vol. 2011, pp. 579–582.
[24] V. V. Nosál, Š. Sivák, and E. K. Konzultanti, "Chronic cerebrospinal venous insufficiency (CCSVI) methodical procedure for the examination of the venous system using ultrasound," *Neurológia*, vol. 5, pp. 163–167, 2010.
[25] D. Centonze, R. Floris, M. Stefanini, S. Rossi, S. Fabiano, M. Castelli, S. Marziali, A. Spinelli, C. Motta, F. G. Garaci, G. Bernardi, and G. Simonetti, "Proposed chronic cerebrospinal venous insufficiency criteria do not predict multiple sclerosis risk or severity," *Ann. Neurol.*, vol. 70, pp. 51–58, Jul. 2011.
[26] M. M. Ciccone, A. I. Galeandro, P. Scicchitano, A. Zito, M. Gesualdo, M. Sassara, F. Cortese, A. Dachille, R. Carbonara, F. Federico, P. Livrea, and M. Trojano, "Multigate quality doppler profiles and morphological/hemodynamic alterations in multiple sclerosis patients," *Curr. Neurovasc Res.*, Apr. 2012.
[27] P. Tortoli, S. Ricci, F. Andreuccetti, and L. Forzoni, "Detection of chronic cerebrospinal venous insufficiency through multigate quality doppler profiles," in *Proc. 2010 IEEE Int. Ultrasonics Symp. (IUS)*, Oct. 2010, pp. 1190–1193.
[28] E. Menegatti, V. Genova, M. Tessari, A. M. Malagoni, I. Bartolomei, M. Zuolo, R. Galeotti, F. Salvi, and P. Zamboni, "The reproducibility of colour Doppler in chronic cerebrospinal venous insufficiency associated with multiple sclerosis," *Int. Angiol.*, vol. 29, pp. 121–126, Apr. 2010.
[29] P. Zamboni and R. Galeotti, "The chronic cerebrospinal venous insufficiency syndrome," *Phlebology*, vol. 25, pp. 269–279, Dec. 2010.
[30] D. H. Miller, F. Barkhof, I. Berry, L. Kappos, G. Scotti, and A. J. Thompson, "Magnetic resonance imaging in monitoring the treatment of multiple sclerosis: Concerted action guidelines," *J. Neurol. Neurosurg. Psychiatry*, vol. 54, pp. 683–688, Aug. 1991.
[31] S. De Beni, M. Macciò, and F. Bertora, "Multimodality navigation tool 'Navigator'," in *Proc. IEEE SICE 2nd Int. Symp. Measurement, Analysis and Modeling of Human Functions*, Genova, Italy, Jun. 2004.
[32] P. Zamboni, E. Menegatti, L. Pomidori, S. Morovic, A. Taibi, A. M. Malagoni, A. L. Cogo, and M. Gambaccini, "Does thoracic pump influence the cerebral venous return?," *J Appl Physiol.*, vol. 112, pp. 904–910, 2012.
[33] E. M. Haacke, Y. Xu, Y. C. Cheng, and J. R. Reichenbach, "Susceptibility weighted imaging (SWI)," *Magn. Reson. Med.*, vol. 52, pp. 612–618, Sep. 2004.
[34] S. Mittal, Z. Wu, J. Neelavalli, and E. M. Haacke, "Susceptibility-weighted imaging: Technical aspects and clinical applications, part 2," *AJNR Amer. J. Neuroradiol.*, vol. 30, pp. 232–252, Feb. 2009.
[35] P. Coupé, P. Hellier, X. Morandi, and C. Barillot, "3D rigid registration of intraoperative ultrasound and preoperative mr brain images based on hyperechogenic structures," *Int. J. Biomed. Imag.*, 2012, 10.1155/2012/531319.
[36] L. Mercier, R. F. Del Maestro, K. Petrecca, A. Kochanowska, S. Drouin, C. X. Yan, A. L. Janke, S. J. Chen, and D. L. Collins, "New prototype neuronavigation system based on preoperative imaging and intraoperative freehand ultrasound: System description and validation," *Int. J. Comput. Assist. Radiol. Surg.*, vol. 6, pp. 507–522, Jul. 2011.
[37] D. C. Nikas, A. Hartov, K. Lunn, K. Rick, K. Paulsen, and D. W. Roberts, "Coregistered intraoperative ultrasonography in resection of malignant glioma," *Neurosurg. Focus*, vol. 14, p. e6, 2003.
[38] L. Forzoni, S. D'Onofrio, S. De Beni, M. M. Laganà, V. Kolev, G. Baselli, G. Ciuti, and D. Righi, "Virtual navigator tridimensiional panoramic imaging in transcranial application," *Biomed Tech*, vol. 57, no. Suppl. 1, 2012, 10.1515/bmt-2012-4282.

Maria Marcella Laganà was born in 1982 and is a Biomedical Engineer. She received the M.Sc. degree in Biomedical Engineering cum laude in 2006 and Ph.D. in Bioengineering (2010), at Politecnico di Milano. She has been collaborating with the Fondazione Don Gnocchi since 2005, working on quantitative Magnetic Resonance Imaging (MRI) for clinical studies of neurological disorders. Research interests: processing conventional and advanced structural MRI of the brain and spinal cord, processing of Susceptibility Weighted Images (learnt at MRI Institute for biomedical research, Detroit, MI, USA, mentored by Prof. M. Haacke), multimodal evaluation of vessel anatomy and hemodynamic.

Maria Giulia Preti is a Ph.D. student in Bioengineering at Politecnico di Milano, received the M.S. degree in Biomedical Engineering cum laude from Politecnico di Milano in 2009. During her Ph.D. (2010–2012), she has been collaborating with the Fondazione Don Gnocchi, Milan. In 2011, she was awarded a Progetto Rocca fellowship from *MIT-Italy* to spend a visiting research period at the MIT, Boston (USA), collaborating with the Center for Morphometric Analysis, MGH, Harvard Medical School. Her current research aims at understanding the connections between brain functionality and brain microscopic anatomy by using advanced techniques of Magnetic Resonance Imaging.

Leonardo Forzoni is a Biomedical Engineer and a Product Manager for portable and mid-range ultrasound systems and phased array probes at Esaote S.p.A. Topics of research interest: advanced multigate Doppler technologies, multimodality fusion imaging, real-time ultrasound image quality enhancement and development of emerging technologies with clinical applications (vascular-arteries and veins-, neurology, obstetrics, adult and pediatric cardiology), design of ultrasound systems user interfaces and their evaluation with respect to the ergonomic issues related to sonography.

Sara D'Onofrio was born in Novara, Italy, in 1975. She is a Biomedical Engineer and received the Degree in Biomedical Engineering at the Politecnico di Milano, Italy; then she was a researcher for 3 years at Fondazione Don Gnocchi, Milan, Italy. After 6 years of activity as Product Manager for an Italian company, acting on PACS system and software for quantitative measurement of vertebral deformities in the prevention of bone affecting disorders, she became Clinical Application Specialist for Ultrasound systems at Esaote, working in the Operational Marketing department. Topics of research interest are advanced multigate Doppler technologies, multimodality fusion imaging, and real-time ultrasound image quality enhancement.

Stefano De Beni is an Electronic Engineer and a Product Manager for High-end ultrasound systems and mini-invasive percutaneous interventional solutions at Esaote S.p.A. Main research tasks: development of innovative solutions regarding ultrasound fusion imaging, elastosonography and biopsy technologies.

Antonello Barberio was born in 1985. He received the B.S. Degree in Radiologic techniques, imaging and radiotherapy in 2009. He has been working at the Radiodiagnostic department at Fondazione Don Carlo Gnocchi since 2010. Research interests: neurological diseases, vascular imaging, vessel morphologic 3D reconstruction with Magnetic Resonance (MR) and Computed Tomography, flow quantification with MR.

Pietro Cecconi was born in 1953. he received the Medical School Degree in 1978 and Residency Diploma in radiology (1983), at University of Milan, Italy. He was a Radiologist at Sant'Anna Hospital (Como, Italy) (1981–1998) and at San Giuseppe (Milan, Italy) (1998–2008). He has been Head of Radiodiagnostic department at Fondazione don Carlo Gnocchi, Milan since 2009. His research interests are in the field of neurodegenerative and cerebrovascular disease investigation with MR and Ultrasound.

Giuseppe Baselli was born in Milano, Italy, in 1958 and received the M.Sc. degree (cum laude) in Electronic Engineering at the Politecnico di Milano, in 1983. Then, he was an assistant professor at the Università di Brescia. He was an Associate professor (1998) and next full professor (2001) at Politecnico di Milano. He was director of the Biomedical Engineering program (2004–2009) and of the Department of Bioengineering (2010–2012) and member of the Academic Senate. His teaching activity is in the fields of bioengineering for physiological control systems and neurosensory systems, biomedical signal processing and modeling, advanced medical imaging. His research interests are in the field of biomedical signal processing and in its relationships with the linear and non-linear modeling of cardiovascular regulation, image reconstruction in oncology and molecular imaging, neuro-imaging and the relationships with brain vascular regulation.